Atmospheric Environment 174 (2018) 99–111

Contents lists available at ScienceDirect

Atmospheric Environment

journal homepage: www.elsevier.com/locate/atmosenv

Isotopic source signatures: Impact of regional variability on the $\delta^{13}CH_4$ trend and spatial distribution

Aryeh I. Feinberg[a,b,*], Ancelin Coulon[a], Andrea Stenke[a], Stefan Schwietzke[c,d], Thomas Peter[a]

[a] Institute for Atmospheric and Climate Science, ETH Zurich, Switzerland
[b] Institute of Biogeochemistry and Pollutant Dynamics, ETH Zurich, Switzerland
[c] Cooperative Institute for Research in Environmental Sciences, University of Colorado, Boulder, CO, USA
[d] NOAA Earth System Research Laboratory, Global Monitoring Division, Boulder, CO, USA

GRAPHICAL ABSTRACT

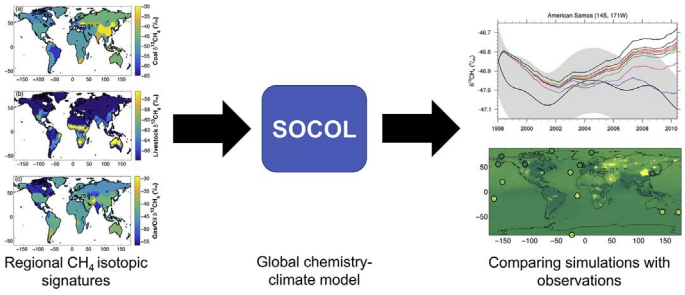

ARTICLE INFO

Keywords:
Methane trends
Methane isotopes
Isotopic signatures
Chemistry-climate model

ABSTRACT

The atmospheric methane growth rate has fluctuated over the past three decades, signifying variations in methane sources and sinks. Methane isotopic ratios ($\delta^{13}CH_4$) differ between emission categories, and can therefore be used to distinguish which methane sources have changed. However, isotopic modelling studies have mainly focused on uncertainties in methane emissions rather than uncertainties in isotopic source signatures. We simulated atmospheric $\delta^{13}CH_4$ for the period 1990–2010 using the global chemistry-climate model SOCOL. Empirically-derived regional variability in the isotopic signatures was introduced in a suite of sensitivity simulations. These simulations were compared to a baseline simulation with commonly used global mean isotopic signatures. We investigated coal, natural gas/oil, wetland, livestock, and biomass burning source signatures to determine whether regional variations impact the observed isotopic trend and spatial distribution. Based on recently published source signature datasets, our calculated global mean isotopic signatures are in general lighter than the commonly used values. Trends in several isotopic signatures were also apparent during the period 1990–2010. Tropical livestock emissions grew during the 2000s, introducing isotopically heavier livestock emissions since tropical livestock consume more C_4 vegetation than midlatitude livestock. Chinese coal emissions, which are isotopically heavy compared to other coals, increase during the 2000s leading to higher global values of $\delta^{13}CH_4$ for coal emissions. EDGAR v4.2 emissions disagree with the observed atmospheric isotopic trend for almost all simulations, confirming past doubts about this emissions inventory. The agreement between the modelled and observed $\delta^{13}CH_4$ interhemispheric differences improves when regional source signatures are used. Even though the simulated results are highly dependent on the choice of methane emission

* Corresponding author. Institute for Atmospheric and Climate Science, ETH Zurich, Switzerland.
E-mail address: aryeh.feinberg@env.ethz.ch (A.I. Feinberg).

https://doi.org/10.1016/j.atmosenv.2017.11.037
Received 27 July 2017; Received in revised form 18 November 2017; Accepted 22 November 2017
Available online 01 December 2017

inventories, they emphasize that the commonly used global mean signatures are inadequate. Regional isotopic signatures should be employed in modelling studies that try to constrain methane emission inventories.

1. Introduction

Due to its significance in climate studies and atmospheric chemistry, methane (CH_4) warrants extensive scientific attention. CH_4 is the second most important anthropogenic greenhouse gas after carbon dioxide (CO_2), with a Global Warming Potential (GWP) of 32 over a 100 year period (Etminan et al., 2016). CH_4 also alters the oxidative capacity of the atmosphere by reacting with hydroxyl (OH) radicals, impacting the lifetime of other airborne compounds (Hartmann et al., 2013). CH_4 emission reductions could help mitigate climate change in the near-term, as the relatively short lifetime of CH_4 will lead to more immediate decreases in radiative forcing compared to CO_2 (Kirschke et al., 2013). For reliable future predictions of climate, the past behavior of atmospheric CH_4 must be better understood.

The growth rate of CH_4 was highly variable in the recent past: decelerating during the 1980s and 1990s, stabilizing at zero growth between 1999 and 2006, and increasing again after 2007 (Kirschke et al., 2013; Nisbet et al., 2016; Saunois et al., 2016). Much of the recent CH_4 research has focused on the changes in CH_4 sources and sinks that led to this growth rate pattern (e.g. Rigby et al., 2017; Turner et al., 2017).

Multiple studies have used stable isotopes to decipher the mechanisms behind the inter-annual variability of CH_4 emissions and sinks (Monteil et al., 2011; Kai et al., 2011; Levin et al., 2012; Nisbet et al., 2014; Ghosh et al., 2015; Schaefer et al., 2016; Schwietzke et al., 2016; Nisbet et al., 2016). The isotopic ratio ($^{13}C/^{12}C$) of CH_4 emitted to the atmosphere varies for different sources. The variation in the emitted CH_4 isotopic ratio depends on three factors: the isotopic ratio of the initial source material (e.g. dissolved CO_2 in a wetland), fractionation during the production process (e.g. methanogenesis by bacteria in the wetland), and whether/how much oxidation occurs before the CH_4 is emitted to the atmosphere (e.g. CH_4 is partly oxidized in the topsoil of the wetland before emission) (Gros et al., 2004; Fisher et al., 2017). The CH_4 source categories have different (yet overlapping) ranges of isotope ratios, with pyrogenic CH_4 (e.g. biomass burning) being the heaviest source for carbon isotopes, then thermogenic sources (e.g. extraction of certain fossil fuels), and lastly biogenic CH_4 (e.g. microbes in wetlands, livestock, etc.) (Kirschke et al., 2013). The chemical sinks of CH_4 also alter the atmospheric CH_4 isotope ratio due to distinct isotopologue reactivities. Heavier isotopologues react slower than their lighter counterparts; sinks thus lead to an enrichment of the heavier isotopologues in the atmosphere. Measurements of the CH_4 isotopic ratios can provide insight into changes in the CH_4 sources and sinks.

The intensified CH_4 growth after 2007 coincided with a global decrease in $\delta^{13}CH_4$ (White et al., 2017). Several studies therefore attribute the CH_4 increase to biogenic sources: augmented wetlands emissions (Dlugokencky et al., 2009, 2011; Bousquet et al., 2011; Bloom et al., 2010; Kirschke et al., 2013; Nisbet et al., 2014, 2016) or agricultural emissions in the tropics (Patra et al., 2016; Schaefer et al., 2016; Nisbet et al., 2016). Nevertheless, others suggest that fossil fuels contributed to the post-2007 CH_4 growth, through increased Asian coal mining emissions or expanded shale gas exploitation by the United States (Kirschke et al., 2013; Bergamaschi et al., 2013; Hausmann et al., 2016; Rice et al., 2016). The interpretation of the CH_4 isotopic record is central in the attempts to explain the recent CH_4 increase.

Past modelling studies have mostly used global mean isotopic signatures, with little consideration of regional variability in the signatures. As well, the published global mean isotopic signatures are based on limited data and may not be accurate (Zazzeri et al., 2016; Schwietzke et al., 2016). Empirical data has underlined the variability of isotopic signatures. For example, the commonly used coal CH_4 signature of − 35‰ is valid only for anthracite coal; lower rank coal can be lighter by up to 30‰. Additionally, coal mined at the surface emits lighter CH_4 than deeper coal, due to biogenic CH_4 that is produced after water incursions (Zazzeri et al., 2015, 2016). Natural gas/oil CH_4 emissions can also vary in their isotopic signatures (Sherwood et al., 2016). Biomass burning and livestock CH_4 isotopic ratios depend on whether C_3 or C_4 vegetation is being burned or consumed (Rust, 1981; Lassey et al., 2007). The C_3 and C_4 photosynthetic pathways discriminate against ^{13}C differently, leading to distinct carbon isotopic compositions in C_3 and C_4 vegetation (Still et al., 2003). Wetland-emitted CH_4 becomes lighter at high latitudes (Gros et al., 2004; Tyler et al., 2007). This could be due to less CH_4 oxidation in high latitude wetlands, distinct methanogenic communities, changes in temperature, and the parent plant material in boreal wetlands being isotopically lighter (C_3) than in tropical wetlands, where C_4 vegetation is also present (Brownlow et al., 2017). Regional changes in emissions could be responsible for the post-2007 CH_4 increase, such as Asian coal mining or tropical wetlands (Nisbet et al., 2014, 2016). Therefore, an effort should be made to accurately represent the source signatures in these regions.

Table 1
Databases used for methane emission fluxes. Global average emissions are shown after scaling (see text).

Source category	Database	Time period	2000–2009 global average (Tg yr^{-1})	Reference
Anthropogenic	EDGAR v4.2	1990–2010	349	EDGAR (2011)
Biomass burning	RETRO[a]	1990–1997	23	Schultz and Rast (2007)
	GFED[b] v3	1997–2010		Randerson et al. (2012)
Wetlands	LPJ-WSL[c]	1990–2010	213	Hodson et al. (2011), Zhang et al. (2016)
Rice	LPJ-WSL	1990–2010	39	Hodson et al. (2011)
Oceans	TransCom-CH_4	climatology	9	Lambert and Schmidt (1993), Patra et al. (2011)
Termites	TransCom-CH_4	climatology	25	Fung et al. (1991), Patra et al. (2011)
Wild animals	TransCom-CH_4	climatology	6	Houweling et al. (1999)
Mud volcanoes	TransCom-CH_4	climatology	7	Etiope and Milkov (2004), Patra et al. (2011)

[a] REanalysis of the TROpospheric chemical composition over the past 40 years.
[b] Global Fire Emissions Database.
[c] Lund-Potsdam-Jena – Swiss Federal Institute for Forest, Snow and Landscape Research.

Table 2
Isotopic ratios ($\delta^{13}CH_4$) and fractionation factors (α_{13C}) used in the BASE simulation.

Source	$\delta^{13}CH_4$ (‰)	Reference
Wetlands	−59	Monteil et al. (2011)
Oceans	−59	Monteil et al. (2011)
Mud volcanoes	−40	Monteil et al. (2011)
Termites	−57	Monteil et al. (2011)
Animals/Livestock	−62	Monteil et al. (2011)
Biomass burning	−21.8	Monteil et al. (2011)
Landfills/waste	−55	Monteil et al. (2011)
Rice	−63	Monteil et al. (2011)
Coal	−35	Monteil et al. (2011)
Oil and gas	−40	Monteil et al. (2011)
Sink	$\delta^{13}CH_4$ (‰)	Reference
Soil	−69	See text
Sink	α_{13C}	Reference
OH	0.9961	Saueressig et al. (2001)
$O(^1D)$	0.9872	Saueressig et al. (2001)
Cl	0.9381	Crowley et al. (1999)

We will address the sensitivity of atmospheric $\delta^{13}CH_4$ to source signatures through a forward-modelling study. We use the state-of-the-art chemistry-climate model (CCM) SOCOL (modelling tools for studies of SOlar Climate Ozone Links) (Stenke et al., 2013). As the model includes CH_4 emission fluxes from different source categories, we can implement regionally varying representations of CH_4 source signatures. Source signatures are investigated for their impact on the spatial distribution and temporal trend during the years 2000–2009.

2. Data and methods

2.1. Model description

SOCOLv3 (Stenke et al., 2013) is a global CCM based on the middle atmosphere version of ECHAM5 (Roeckner et al., 2003), the fifth generation of the European Centre/HAMburg general circulation model (GCM), and the chemical transport model (CTM) MEZON (Egorova et al., 2003). ECHAM5 is coupled to MEZON through the distribution of temperature and radiation-active chemical species. The model is run in T42 horizontal resolution (2.8° × 2.8°~) and 39 vertical levels up to around 80 km. Tracer advection is based on a flux-form semi-Lagrangian scheme (Lin and Rood, 1996). The model time-step is 15 min for dynamics and 2 h for chemistry and radiation. For the years 1990–2010 the model was run with specified dynamics ("nudging"), a relaxation technique that forces the model dynamics towards ERA-Interim reanalysis data (Dee et al., 2011). This reduces the influence of model dynamics on the comparison between observed and simulated isotope ratios. SOCOL includes detailed stratospheric and tropospheric background chemistry, including the oxidation of CH_4 by OH, $O(^1D)$, and Cl. The chemistry scheme also contains the Mainz isoprene mechanism (MIM-1) (Pöschl et al., 2000). More information about the SOCOL version used in this study can be found in Revell et al. (2015).

2.2. CH_4 emission fluxes

The model simulations presented here use a flux boundary condition for CH_4 (i.e. emission fluxes). Estimates of CH_4 emissions from different source categories were employed (Table 1). As well, the CH_4 soil sink was calculated online using uptake maps from Spahni et al. (2011), scaled by simulated atmospheric CH_4 concentrations.

The tropospheric OH concentrations in SOCOL are likely too high (Revell et al., 2015; Coulon, 2016), leading to a shorter atmospheric CH_4 lifetime than in reality. Coulon (2016) evaluated the simulated methyl chloroform (MCF) trend against observations, as MCF can be used as a tracer of OH variability (Montzka et al., 2011). The evaluation demonstrated that simulated tropospheric OH is high biased by 27% for 1997–2008; however the offset from observations is constant. Therefore, in our simulations OH should not distort the CH_4 and $\delta^{13}CH4$ trends. However, since the OH sink varies spatially, the spatial distribution of the isotopic ratio may be impacted by this error. As well, SOCOL simulates 40% higher OH in the NH troposphere than the SH. Estimates constrained by MCF measurements suggest that the ratio is closer to unity (Patra et al., 2014). Since the OH interhemispheric ratio is similar in all simulations, this bias would be consistent throughout the study.

In order to compensate for the high OH bias, CH_4 emissions in Table 1 were scaled by 1.23 to yield the observed global mean CH_4 concentration in 1980. The combination of bottom-up estimates of different source categories may lead to an unrealistic value for total CH_4 emissions, so applying scaling factors to emissions is common in other modelling studies (Monteil et al., 2011; Patra et al., 2011; Ghosh et al., 2015). The total scaled CH_4 emissions from 2000 to 2009 in the simulation (671 Tg $CH_4 yr^{-1}$) agree with the Kirschke et al. (2013) estimate for total bottom-up emissions (678 Tg $CH_4 yr^{-1}$). The emission weighted average isotopic signature of CH_4 for each simulation is not affected by scaling the emissions.

2.3. Isotopic implementation

Since deviations of isotopic ratios from the standard ratio are usually small, they are often reported in $\delta^{13}CH4$ notation:

$$\delta^{13}CH_4 = \left(\frac{[^{13}CH_4][[^{12}CH_4]]}{^{13}R_{VPDB}} - 1 \right) \times 1000‰ \quad (1)$$

where R_{VPDB} is the isotope ratio of the Vienna Pee Dee Belemnite (VPDB) standard ($^{13}C/^{12}C$ = 0.0112372). For chemical reactions, differences in the rate constants (k) between $^{12}CH_4$ and $^{13}CH_4$ can be described by the fractionation factor, α_{13C} (Allègre and Sutcliffe, 2008):

$$\alpha_{13C} = \frac{^{13}k}{^{12}k} \quad (2)$$

Isotopic fractionation is sometimes represented by ε_{13C} notation, also called the kinetic isotope effect:

$$\varepsilon_{13C} = (\alpha_{13C} - 1) \times 1000 \quad (3)$$

For a baseline simulation (BASE), we selected the global mean source signatures in Table 2, which are commonly used in modelling studies (e.g. Monteil et al., 2011; Ghosh et al., 2015; Coulon, 2016). Global mean CH_4 emissions have an isotopic signature of around − 53‰. The chemical sinks of CH_4, by preferentially removing the lighter isotope of CH_4, shift the isotopic ratio by + 6‰ to yield the observed atmospheric $\delta^{13}CH_4$ (~ −47‰). It is important to note, however, that the equilibration timescale of atmospheric $\delta^{13}CH_4$ is long and the observed atmospheric $\delta^{13}CH_4$ may lag changes in CH_4 emissions and sinks (Tans, 1997).

The fractionation factors for the OH, $O(^1D)$, and Cl reactions were compiled from the literature (Table 2). In addition to acting as a stratospheric oxidant of CH_4, atomic Cl has been suggested to act as a sink for CH_4 in the marine boundary layer (Allan et al., 2007). This could influence the variability of $\delta^{13}CH_4$ due to the strong isotopic fractionation effect of Cl. However, the SOCOL model does not include a parametrization for atomic Cl production in marine environments. We decided that inclusion of this sink is out of the scope of this study since the spatial distribution and inter-annual variability of marine Cl are highly uncertain. The soil sink was implemented as a negative source that removes CH_4 at the surface. The isotopic fractionation from soil is

expressed in $\delta^{13}CH_4$ notation, similar to sources (Allan et al., 2001). The ε_{13C} due to soil fractionation was measured to be − 22 ‰ (Snover and Quay, 2000). The effective soil $\delta^{13}CH_4$ was assigned by depleting the atmospheric $\delta^{13}CH_4$ (∼ −47 ‰) by the soil ε_{13C} (− 47 − 22 = −69 ‰).

2.4. Simulations setup

Initial conditions were produced by spinning up the model for 15 years under 1990 conditions. As shown by Tans (1997), CH_4 isotopic ratios take longer to equilibrate after perturbations than total CH_4. The 15 year spin-up time was sufficient for the isotopic ratio to be equilibrated in the troposphere. A spin-up was performed for each simulation, to ensure that the isotopes were equilibrated with the isotopic source signatures of that particular simulation.

Variability in five source signatures was investigated: coal, natural gas/oil, wetlands, livestock, and biomass burning (Table 3). The implemented spatial distribution of these source signatures will be described below. The use of regional source signatures leads to a more flexible global average source signature that changes over the course of the simulation, as the emissions from different regions change (Fig. 4). Assuming that the source signature distributions that we applied are correct, this should lead to a more accurate trend in atmospheric $\delta^{13}CH_4$.

2.4.1. Coal $\delta^{13}CH_4$

In addition to BASE, another simulation was run with a globally constant coal source signature: L-COAL with a recently suggested global mean of −50‰ (Zazzeri et al., 2016). As a first method to introduce regional differences in coal $\delta^{13}CH_4$, in M-COAL country-level coal production statistics were used. Zazzeri et al. (2016) assigned different source signatures to anthracite coal mined underground ($\delta^{13}C_a^u = -30‰$), anthracite mined at the surface ($\delta^{13}C_a^s = -40‰$), bituminous to sub-bituminous coal mined underground ($\delta^{13}C_{sb}^u = -55‰$), and bituminous to sub-bituminous coal mined at the surface ($\delta^{13}C_{sb}^s = -65‰$). We also assumed that lignite coal would correspond to these bituminous to sub-bituminous values, as Kanduč et al. (2015) measured a similar mean value for $\delta^{13}CH_4$ (− 54.5 ‰) from lignite coal mined underground. The coal isotopic signature for a country ($\delta^{13}C_{coal}$) can then be calculated using the following equation:

$$\delta^{13}C_{coal} = x_a^u \delta^{13}C_a^u + x_a^s \delta^{13}C_a^s + x_{sb}^u \delta^{13}C_{sb}^u + x_{sb}^s \delta^{13}C_{sb}^s \quad (4)$$

where x_a^u is the fraction of the country's coal production that is underground anthracite, x_a^s is the fraction of surface anthracite, x_{sb}^u is the fraction of underground sub-bituminous coal, and x_{sb}^s is the fraction of surface sub-bituminous coal. For the 21 highest coal producing countries, we obtained data for the fraction of coal mined underground versus at the surface (Schwietzke et al., 2014; Euracoal, 2011). These countries account for around 90% of coal emissions in EDGAR v4.2 for 2000–2010. As well, the World Energy Council (2007) provides country-level data for the fraction of total coal production in 2005 that is bituminous (including anthracite), sub-bituminous, or lignite coal. We assume that the reported fraction of bituminous coal is completely anthracite, and add the lignite coal fraction to the sub-bituminous category, as they have similar CH_4 isotopic signatures. We also assume that the fractions of mined coal ranks and depths do not change throughout the simulation period. Inputting this data into Equation (4), we can calculate the coal signatures of these 21 countries. The country-level coal mining data that we used is listed in Table S1.

The resultant spatial distribution for coal $\delta^{13}CH_4$ (used in M-COAL) is shown in Fig. 1a. Wherever coal statistics were unavailable, we assumed that the global coal signature is −50‰, as suggested by Zazzeri et al. (2016). We acknowledge that the assignment of coal ranks to specific signatures is based on limited measurements. As well, the country-level data for the fraction of coal mined at the surface vs. underground and the fraction of bituminous vs. sub-bituminous coal may be misreported from some countries. However, this approach does provide an idea of which countries could have heavier or lighter coal emissions, based on the reported rank and depth of mined coal.

Due to the uncertainties in developing a coal $\delta^{13}CH_4$ map, we ran an additional simulation (M-COAL_S) using country-level coal signatures from Schwietzke et al. (2016), based on Sherwood et al. (2016). We can thus test the impact of using different methods to derive the regional coal signature variability. Sherwood et al. (2016) provide 13 countries' coal isotopic signatures based on 1402 empirical samples, by averaging available measurements from coal mines in those countries. These countries account for around 80% of emissions during 2000–2010 in our simulations. Wherever data was unavailable we applied the mean coal signature calculated by Schwietzke et al. (2016), − 43.4 ± 0.8‰ (error is 1 standard deviation). The M-COAL_S coal source signature map is shown in Fig. 1b.

Differences between the coal signature distributions of M-COAL and M-COAL_S are shown in Fig. 1c. For USA and China, the two major coal mining countries, the two methods agree within 5‰. However, other countries show larger deviations. The Turkish coal signature in M-COAL is 21‰ lighter than in M-COAL_S, and the South African coal signature is 17‰ heavier. This could be caused by inaccurate end-members used in the M-COAL calculation of country-level source signatures, or an unrepresentative average in Sherwood et al. (2016) due to a lack of coal signature data. For example, in Turkey the Sherwood et al. (2016) data is based only on one study from the Zonguldak Basin, a hard coal basin (Hosgörmez, 2007). However, Turkey overwhelmingly mines lignite coal (94.5% of total 2005 production), which emits lighter CH_4, meaning that the measurements from this basin are not representative of Turkey (World Energy Council, 2007). We bring up the example of Turkey, even though it was only the 12th top coal producer in the world in 2005 (World Energy Council, 2007), because it illustrates the limitations of extrapolating from single-basin measurements to country-level averages. The M-COAL distribution may be flawed because it is not based on in-situ $\delta^{13}CH_4$ data, whereas the M-COAL_S distribution is limited depending on the number of coal mines in each country that have been sampled. It is therefore interesting to see how these two coal signature maps impact the isotopic trends and spatial distribution.

2.4.2. Wetlands $\delta^{13}CH_4$

We analyzed the available wetland isotopic measurements, including those compiled by Sherwood et al. (2016), to determine whether there is a latitudinal trend in the emitted isotopic CH_4 signature from wetlands (Fig. 2). South of 40° N, there is no significant trend in the wetland-emitted $\delta^{13}CH_4$ (Student's t-test, $p = 0.32$). However, north of 40° N, the wetland $\delta^{13}CH_4$ decreases by around 0.46‰ per degree of latitude. The latitudinal trend in the measured wetland signature north of 40° N is significant ($p = 0.001$). The available data therefore indicates

Table 3
Simulations testing sensitivity to source signatures.

Name	Description
BASE	Source signatures taken from Table 2
L-COAL	A light isotopic coal signature is used globally (− 50‰)
M-COAL	Mapped coal signatures; based on coal rank/depth
M-COAL_S	Mapped coal signatures; based on Sherwood et al. (2016)
M-WET	Latitudinal wetland signature; lighter in northern high latitudes
M-BB	Mapped biomass burning signatures; based on C_3 and C_4 distribution
M-COW	Mapped livestock signatures; based on C_3 and C_4 distribution
M-GAS	Country-level natural gas and oil signatures, based on Sherwood et al. (2016)
M-ALL	All mapped signatures (M-COAL, M-WET, M-BB, M-COW, M-GAS)
M-WET_OFFSET	M-WET, offset to the global mean wetland signature in BASE (− 59‰)
M-COW_OFFSET	M-COW, offset to the global mean wetland signature in BASE (− 62‰)

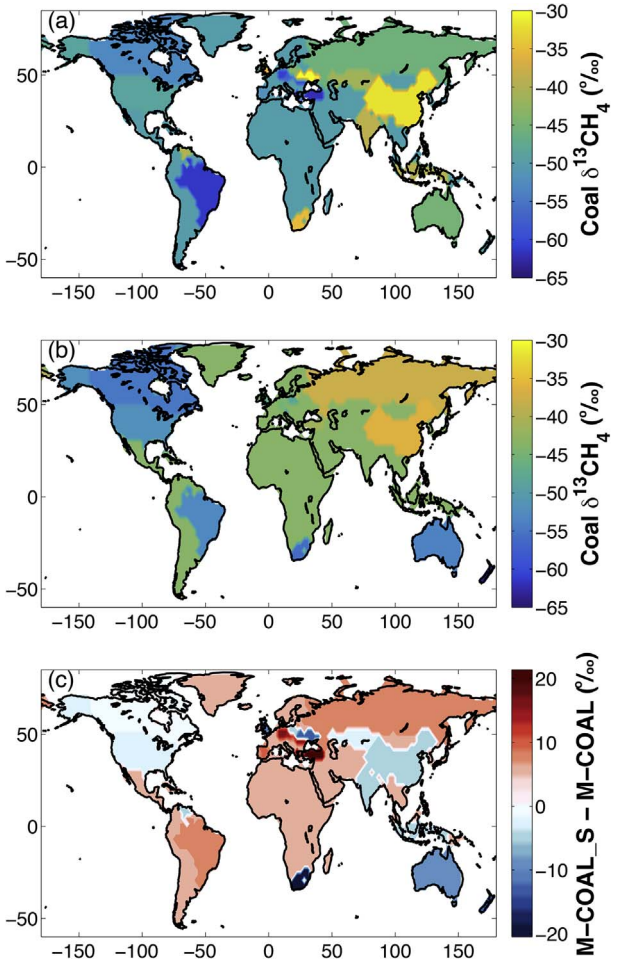

Fig. 1. Different methods of calculating the distribution of coal $\delta^{13}CH_4$. (a) Coal $\delta^{13}CH_4$ in M-COAL, calculated using coal mining statistics (b) Coal $\delta^{13}CH_4$ in M-COAL_S, calculated using empirical data (c) Difference between the two coal signature distributions.

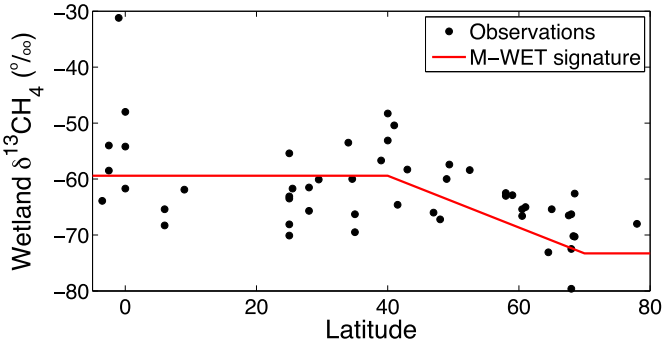

Fig. 2. Latitudinal variation of wetland $\delta^{13}CH_4$ inputted in the M-WET simulation compared to observational studies. The inputted wetland $\delta^{13}CH_4$ is shown as a red line and observational studies are shown as black circles. Observations are taken from numerous studies that measured wetland $\delta^{13}CH_4$. We use the isotopic signature database from Sherwood et al. (2016) and references therein, along with several additional studies (Tyler, 1986; Tyler et al., 1988; Martens et al., 1992; Walter et al., 2006, 2008; Umezawa et al., 2012; McCalley et al., 2014; O'Shea et al., 2014). (For interpretation of the references to colour in this figure legend, the reader is referred to the web version of this article.)

that lighter CH_4 is emitted from boreal wetlands.

We introduced a latitudinally varying wetland isotopic signature in our M-WET simulation. South of 40° N, we used a $\delta^{13}CH_4$ value of − 59.4‰ for wetland emissions, the mean from the data in Fig. 2. Between 40° N and 71° N, we applied the decreasing trend of 0.46‰ per

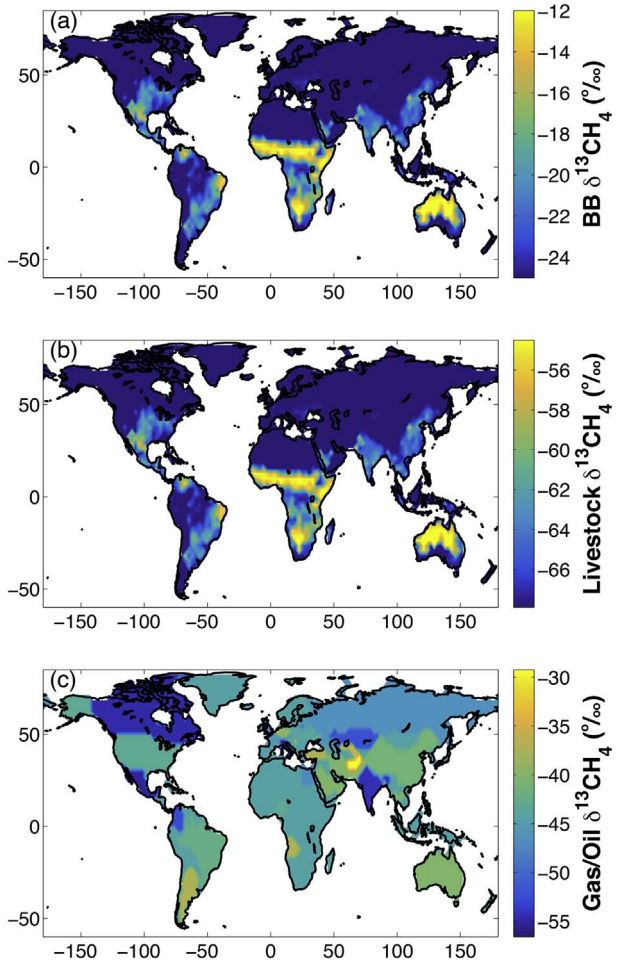

Fig. 3. Maps of CH_4 source signatures (a) Biomass burning $\delta^{13}CH_4$ in M-BB (b) Livestock $\delta^{13}CH_4$ in M-COW (c) Natural gas/oil $\delta^{13}CH_4$ in M-GAS.

degree of latitude. To avoid discontinuities in the wetland signature, the fitted trend in wetland $\delta^{13}CH_4$ between 40° N and 71° N is offset at 40° N to − 59.4‰ (Fig. 2). North of 71° N, the isotopic signature was held constant at − 73.6 ‰, as there are very few measurements of wetland isotopic signatures at these latitudes. The red line is not the only function that could fit the available measurements. However, it is one option for capturing the observation that isotopically lighter emissions occur from boreal wetlands.

2.4.3. *Biomass burning $\delta^{13}CH_4$*

In the simulation M-BB, we assigned C_3 and C_4 biomass burning source signatures of −25‰ and −12‰ according to Lassey et al. (2007) (Dlugokencky et al. (2011), however, suggested values of −26‰ and −17‰ for C_3 and C_4 burning). Still et al. (2003) determined the spatial distribution of the C_4 vegetation fraction using satellite measurements, climatic data, and crop harvest data. The C_4 fraction distribution, after regridding to T42 resolution, was used to calculate a mean biomass burning signature for each grid box. The regional distribution of biomass burning $\delta^{13}CH_4$ is shown in Fig. 3a.

2.4.4. *Livestock $\delta^{13}CH_4$*

We again use the Still et al. (2003) C_4 fraction to calculate regional livestock signatures. We assume that livestock graze or are fed vegetation that corresponds to the local C_3/C_4 ratio. From the studies compiled by Sherwood et al. (2016), the mean emitted isotopic signature of C_3- and C_4- fed livestock is − 67.9‰ and − 54.5‰, respectively. Using these two signatures and the C_4 fraction, we determined the spatial distribution of livestock $\delta^{13}CH_4$ (Fig. 3b). This regional

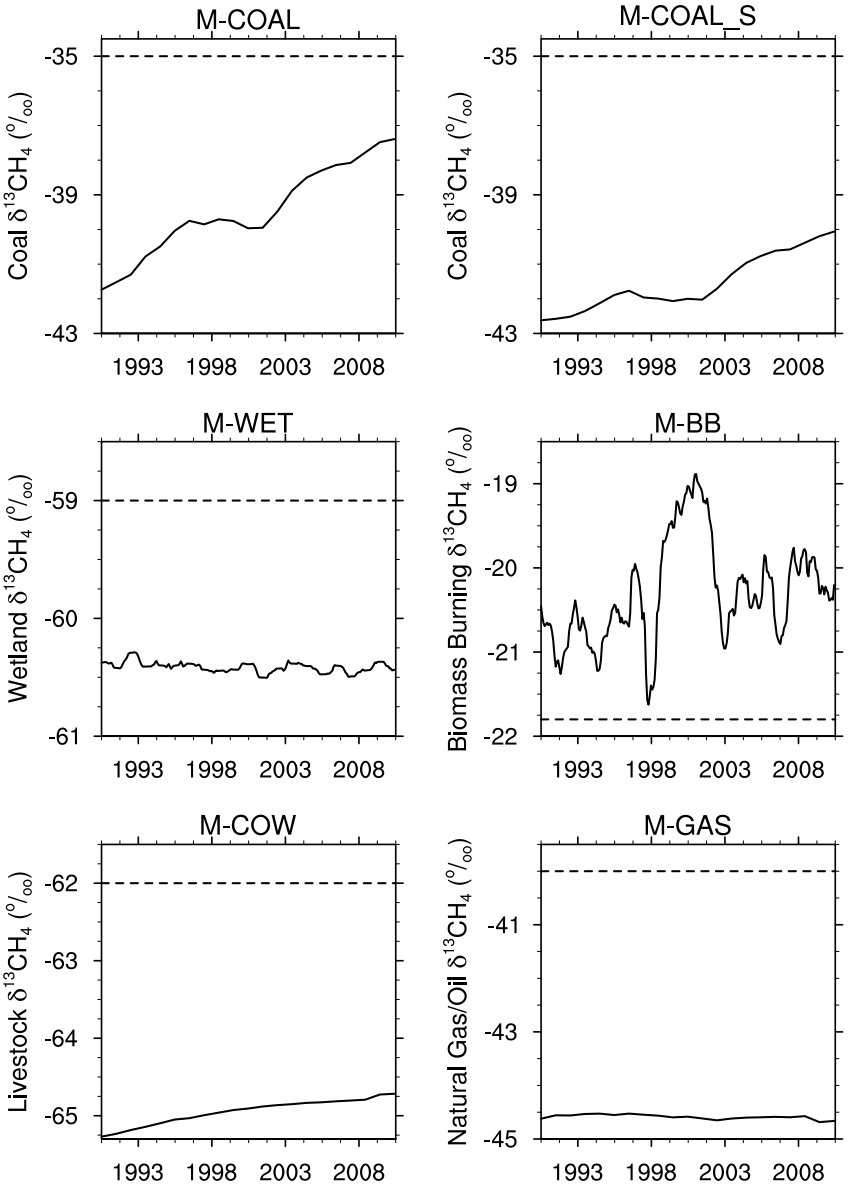

Fig. 4. Trend in global mean source signatures, weighted by CH_4 emissions, throughout the simulations (solid line). Values are smoothed with a 12 month running average. The dotted lines show the commonly used isotopic signatures from the BASE simulation.

variation in the livestock source signature is inputted into the M-COW simulation.

2.4.5. Natural gas/oil $\delta^{13}CH_4$

We use the country-level natural gas/oil $\delta^{13}CH_4$ values from the Sherwood et al. (2016) database, also used in Schwietzke et al. (2016). Data is available for 43 countries, accounting for around 70% of natural gas/oil emissions in EDGAR v4.2 during 2000–2010. We applied the global mean calculated by Schwietzke et al. (2016) (− 44.5 ‰) wherever data were unavailable. The isotopic signature map used for the M-GAS simulation is shown in Fig. 3c.

2.4.6. Offset regional source signatures

In every simulation with regionally varying isotopic source signatures, the global mean isotopic signature is also changed for that source. For example, M-WET shifts the global mean wetland signature from − 59‰ in BASE to around − 60.4‰. Changes in the isotopic spatial distribution and trends can arise from this shift in the mean source signature. In order to investigate the sole effect of regional variability, we removed this global mean shift from the BASE isotopic signature for two additional simulations of wetland and livestock sources. In M-WET_OFFSET the distribution in Fig. 2 was shifted by a constant offset of 1.4‰. The regional variability of the wetland isotopic signature is retained but the global mean is − 59 ‰, the same value as in BASE. Similarly, in M-COW_OFFSET the isotopic source signatures are increased everywhere from M-COW by 2.8‰. This leads to a 2000–2010 global mean livestock signature of − 62 ‰, the BASE value.

2.5. Observations

CH_4 observations were provided by NOAA-ESRL (Dlugokencky et al., 2015). $\delta^{13}CH_4$ observations were measured by INSTAAR at the University of Colorado for 19 of the NOAA-ESRL stations (shown in Fig. 1c), the earliest of which began measuring in 1998 (White et al., 2017). The isotopic measurements will be referred to as NOAA-INSTAAR in this publication. The observations at surface sites were compared with the model grid boxes in which the sites were located. While model tracers are outputted continuously, observations of CH_4 and its isotopologues suffer from irregular sampling periods and prolonged data gaps. We employed a harmonic regression approach on the observations to reduce the influence of these irregularities on the model evaluation (see Section S1). Harmonic regression has often been applied to measurements of atmospheric trace gases (Nakazawa et al., 1997; Levin et al., 2012). Smoothing of simulated quantities was performed using a 12 month running average.

3. Results and discussion

3.1. Transient source signatures

When regional isotopic variations are considered for the CH_4 sources, the global mean source signatures differ from the commonly cited global means (Fig. 4). For all of the sources except biomass burning, the isotopic signatures are globally lighter than the BASE isotopic signature. This confirms the analysis in Schwietzke et al. (2016), who also found that modelling studies use too heavy global isotopic signatures for CH_4 emissions. The previously used isotopic signatures were based on less empirical data than this study and Schwietzke et al. (2016). The lighter $\delta^{13}CH_4$ values calculated by this paper are likely more representative of the actual global mean signatures.

In our simulations the global mean isotopic signatures of source categories vary over time. The contributions of different regions to emissions have changed in previous decades, which is evidenced by several of the source signatures in Fig. 4. The $\delta^{13}CH_4$ of global livestock emissions increases from 1990 to 2010. This is due to the expanding influence of agriculture from tropical regions (India, South America, and Tropical Asia), where heavier C_4 vegetation is more prevalent. The global mean coal source signature becomes heavier over time using both of the coal maps, M-COAL and M-COAL_S. $\delta^{13}CH_4$ of coal emissions increases due to growing Chinese coal emissions, which are relatively heavy (− 36 ‰ in M-COAL_S) compared to the global average (− 42.5 ‰ in 1990). The coal signature trend in M-COAL_S is smaller than in M-COAL, because Chinese coal is 5 ‰ lighter in M-COAL_S. The global mean of biomass burning $\delta^{13}CH_4$ shows a strong decrease during the 1997–1998 El Niño, due to extremely high C_3 burning (Randerson et al., 2005). After 2002 the biomass burning signature is fairly stable (Fig. 4). The global mean source signatures of natural gas/oil and wetland emissions are relatively constant throughout the simulation (Fig. 4). The variation of CH_4 source signatures over time due to changing regional emissions has not been considered in previous modelling studies.

3.2. Simulation of CH_4

We will briefly discuss how simulated CH_4 compares with NOAA-ESRL observations (Dlugokencky et al., 2015). The CH_4 spatial distribution of our simulations agrees quite well with NOAA-ESRL observation stations (Fig. 5). The interhemispheric difference (IHD) will be defined here as the 2001–2010 mean CH_4 concentration at South Pole Observatory (SPO) minus that of Alert, Canada (ALT, 82° N, 62° W). The CH_4 IHD of observations is − 130 ppb, whereas in the simulations it is − 107 ppb. Errors in simulated interhemispheric

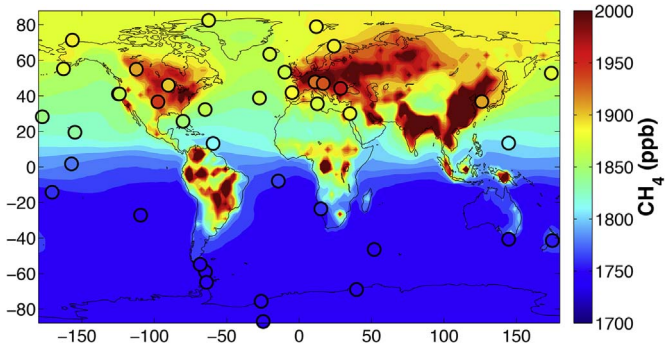

Fig. 5. Spatial distribution of surface CH_4 compared to NOAA-ESRL stations in 2010 (filled circles) (Dlugokencky et al., 2015). Simulated values are offset to Alert, Canada (82° N, 62° W). High altitude stations that do not correspond to the surface model pressure level are not shown. The displayed range of CH_4 does not cover the full range of simulated CH_4, as model boxes with large emissions can have extreme CH_4 values.

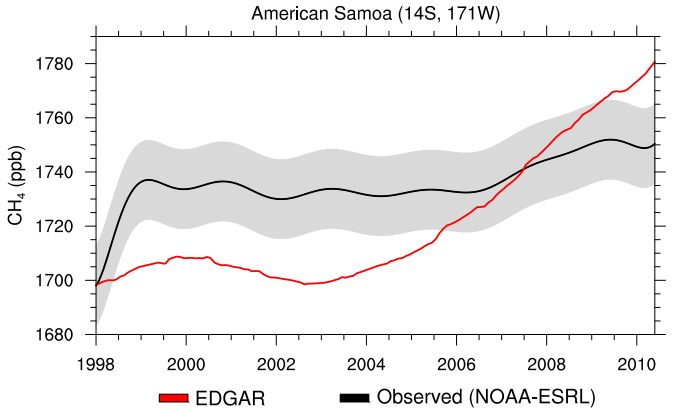

Fig. 6. Deseasonalized simulated CH_4 trend at American Samoa, compared to observations (Dlugokencky et al., 2015). The grey shading shows the 2σ uncertainty range due to fitting error. The simulation is offset to agree with the observations in 1998.

transport are minimized by nudging the model dynamics to ERA-Interim meteorology. Thus the small difference in IHD between simulations and observations is due to incorrect distributions of CH_4 emissions and/or sinks.

At American Samoa (SMO, 14° S, 171° W), our simulations illustrate a constant CH_4 trend from 1998 to 2004, similar to observations (Fig. 6). However, after 2004 the trend in CH_4 concentrations is too high compared to observations. Although only SMO is shown, similar discrepancies between model and observations were observed at other sites. Through source-tracking and isotopic methods, the excessive trend in this period was attributed to the overestimated increase in Chinese coal emissions by EDGAR v4.2 (Coulon, 2016). However, in that study the commonly used global mean signatures (Table 2) were used, which are likely not accurate (Zazzeri et al., 2016; Schwietzke et al., 2016). The EDGAR v4.2 emissions will be evaluated in this study using more accurate isotopic signatures, to assess whether they are compatible with isotopic observations.

3.3. $\delta^{13}CH_4$ trends

NOAA-INSTAAR isotopic measurements show a stable isotopic trend from 2000 to 2008, followed by a decrease after 2008 (White et al., 2017). Fig. 7 compares the observed $\delta^{13}CH_4$ trend with simulated

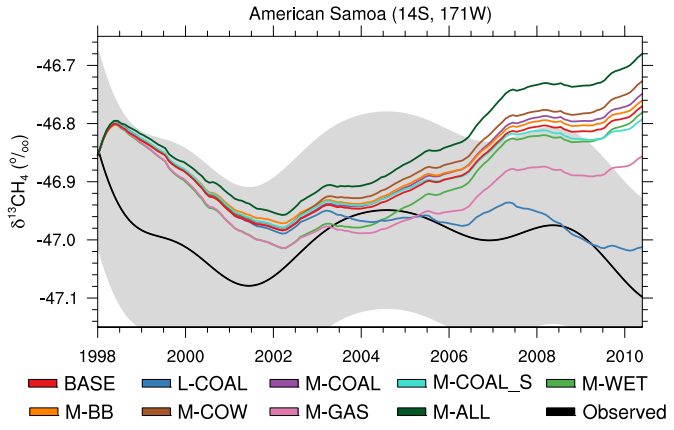

Fig. 7. Comparison of simulated $\delta^{13}CH_4$ concentrations with NOAA-INSTAAR observations at American Samoa (White et al., 2017). Black line shows smoothed deseasonalized observations (harmonic regression) and grey shading shows 2σ uncertainty range due to fitting error. Colored lines represent the deseasonalized simulated CH_4 (12 month running average). A constant offset is applied to each simulation so that they agree with observations in 1998. (For interpretation of the references to colour in this figure legend, the reader is referred to the web version of this article.)

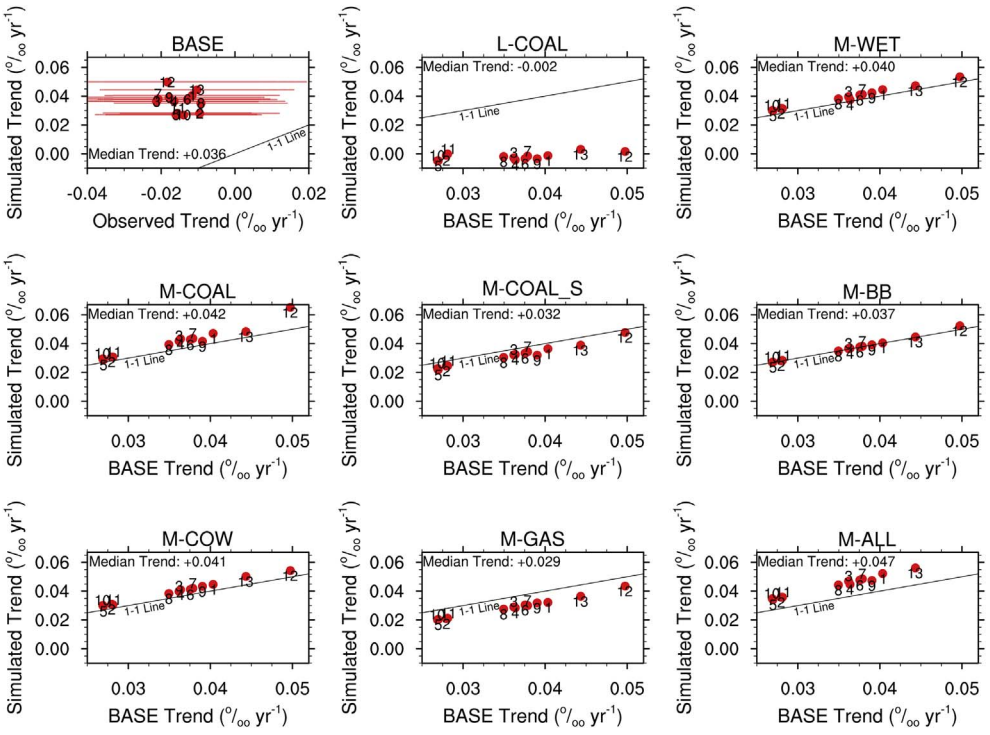

Fig. 8. Summary of simulated and observed $\delta^{13}CH_4$ trends at NOAA-INSTAAR sites between 2003 and 2010 for the sensitivity simulations. BASE trends are compared with observed trends, while the other sensitivity simulations are compared to BASE. Trends were calculated non-parametrically using the Theil-Sen estimator on deseasonalized simulated and observed $\delta^{13}CH_4$. Red lines show the 2σ error interval in the observed trend due to uncertainties in the harmonic regression fitting. The 13 sites shown are the NOAA-INSTAAR sites that began measuring before 2003. Site names corresponding to the site numbers are shown in Table S2. Median simulated trends are listed on the plots. (For interpretation of the references to colour in this figure legend, the reader is referred to the web version of this article.)

Table 4
Comparing the 2003–2010 isotopic trends of M-WET and M-COW (referred to as 'Original simulation' in the table) with M-WET_OFFSET and M-COW_OFFSET (referred to as 'Offset simulation' in the table). The median trend is calculated from 13 NOAA-INSTAAR sites, as in Fig. 8. The BASE trend is also listed for comparison.

CH_4 source	Original simulation trend (% yr^{-1})	Offset simulation trend (% yr^{-1})
Wetlands	+0.040	+0.037
Livestock	+0.041	+0.041
BASE	+0.036	

trends at SMO, a site which should be representative of the background troposphere. The largest difference between the observations and the BASE simulation occurs after 2002. BASE shows a positive $\delta^{13}CH_4$ trend in this period. Fig. 8 shows that the isotopic trend in BASE disagrees with observations at all measurement sites. The Chinese coal emissions increase in EDGAR v4.2 has been suggested to be overestimated (Patra et al., 2011; Bergamaschi et al., 2013; Bruhwiler et al., 2014; Peng et al., 2016). These excessive coal emissions lead to increasingly heavy $\delta^{13}CH_4$ in BASE. Coulon (2016) illustrated with the same CCM that using fossil fuel emissions from Schwietzke et al. (2014) can lead to better agreement with the observed isotopic trend. The impact of changing emission inventories has already been explored by Coulon (2016). Therefore this section will focus on evaluating the simulated isotopic trends under different source signature assumptions, using the same emissions.

Fig. 8 compares the 2003–2010 BASE trend with the trends in the other sensitivity simulations. L-COAL shows a stable isotopic trend, bringing it into agreement with the observations. Coal mining was the cause of the increasingly heavy $\delta^{13}CH_4$ in BASE. In L-COAL the coal emissions are 15 ‰ lighter than in BASE (− 50‰), close to the value of the weighted mean atmospheric CH_4 source signature (~ −53 ‰). Under these conditions, coal emissions no longer exert the same heavy influence on atmospheric $\delta^{13}CH_4$. However, the L-COAL global mean signature of − 50‰ seems unrepresentative of the mean Chinese coal signature based on 195 available measurements, − 36 ‰ (Sherwood et al., 2016), and Chinese coal production increased the most out of any country during the 2000s.

Since global mean coal signatures are unrepresentative in specific regions, we ran two simulations with regionally varying coal isotopic signatures. These two simulations, M-COAL and M-COAL_S, showed very different trends. In M-COAL the median 2003–2010 trend is 17% higher than in BASE at NOAA-INSTAAR sites, whereas in M-COAL_S it is 11% lower (Fig. 8). In M-COAL_S, the global mean coal source signature is lighter than in BASE (− 42‰ in 2000). Similarly to L-COAL, coal emissions have a weaker influence on atmospheric $\delta^{13}CH_4$ when they are lighter. M-COAL also has a lighter global mean coal signature than in BASE (− 40‰ in 2000). However, M-COAL displays a stronger increase in coal $\delta^{13}CH_4$ throughout the simulation (Fig. 4). This is due to Chinese coal being heavier in M-COAL than in M-COAL_S (− 31.8‰ vs. − 36.1‰). The strong trend in coal $\delta^{13}CH_4$ overcomes the overall lighter coal signature in M-COAL, leading to a steeper $\delta^{13}CH_4$ trend than BASE. On the other hand, M-COAL_S is dominated by having a lighter mean coal signature than BASE, leading to a shallower $\delta^{13}CH_4$ trend. The choice of coal map can influence the simulated $\delta^{13}CH_4$ through its global mean value and trend.

The difference in M-COAL and M-COAL_S reveals the inherent uncertainty in constructing source signature maps. The gaps between these approaches could be reduced with further isotopic measurements of coal signatures in countries which have been undersampled. The $\delta^{13}CH_4$ of Chinese coal emissions is clearly an important parameter in understanding past CH_4 changes. However, special attention should also be paid to countries that are projected to increase coal emissions in the future. Due to its rapid economic development and booming population, Southeast Asia is expected to nearly double its energy consumption by 2035. This energy will mainly be provided through increased coal combustion (Zhu, 2013; IEA, 2015; Koplitz et al., 2017). There have been no reported measurements of coal $\delta^{13}CH_4$ in Indonesia or Vietnam, the two top coal producers in the region (Sherwood et al., 2016). Therefore measurements of coal $\delta^{13}CH_4$ in this region will be invaluable for diagnosing future CH_4 changes.

In M-WET the isotopic trend is 11% higher than BASE. However, with the M-WET_OFFSET simulation we can test whether this trend is increased solely due to the shift in the global mean wetland signature.

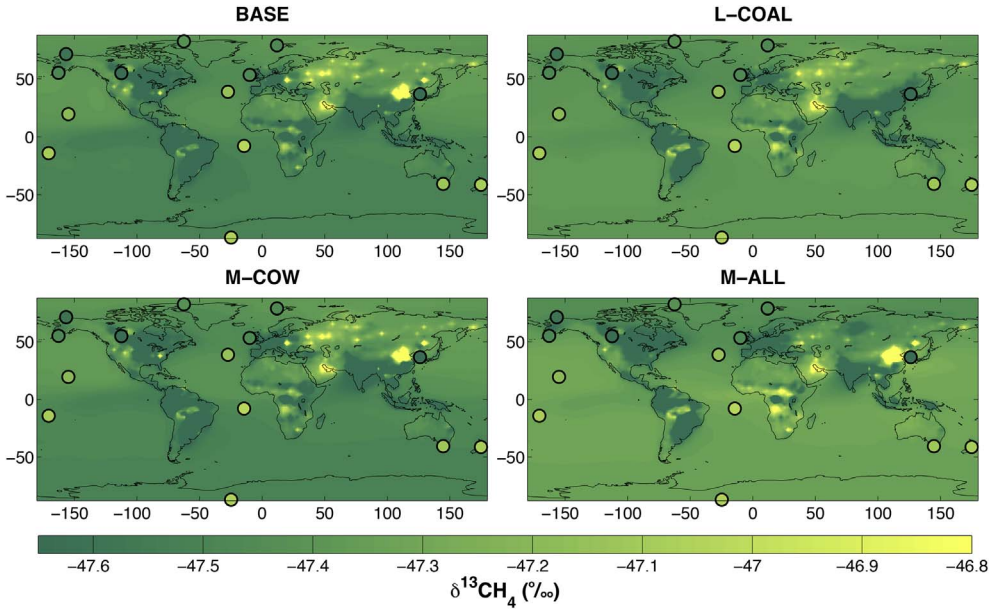

Fig. 9. Simulated annual mean surface $\delta^{13}CH_4$ in 2010, compared to NOAA-INSTAAR stations (filled circles) (White et al., 2017). Only 4 simulations are shown, the remaining simulations are displayed in Fig. S2. Simulated values are offset to agree with the Alert, Canada (ALT) annual mean.

In Table 4, we can see that M-WET_OFFSET shows a similar trend to BASE. Therefore M-WET only has a steeper trend because the global mean wetland isotopic signature is lighter than in BASE (Fig. 4). Wetlands become a less important CH_4 source between 2001 and 2010, as coal emissions rapidly increase in our simulations. When the wetlands fraction of total CH_4 emissions decreases in M-WET, the isotopic trend is higher than BASE because a slightly lighter emission source is lost.

In M-COW the isotopic trend is increased by 14% from BASE. This is caused by the increasing trend in the livestock isotopic signature (Fig. 4), driven by larger livestock emissions from tropical regions with higher C_4 vegetation fractions. As opposed to M-WET, the shift in the global mean livestock signature from BASE does not influence results. Both M-COW and M-COW_OFFSET show similar isotopic trends (Table 4). Thus the increasing $\delta^{13}CH_4$ trend of livestock emissions drives a stronger simulated atmospheric $\delta^{13}CH_4$ trend. Other studies have suggested that the observed post-2008 decrease in $\delta^{13}CH_4$ is at least partly due to increasing livestock emissions in tropical South America, Africa, and Asia (Patra et al., 2016; Schaefer et al., 2016; Nisbet et al., 2016). It is important to consider that these tropical livestock emissions are isotopically heavier, meaning that a larger increase in livestock emissions is necessary to explain the observed $\delta^{13}CH_4$ decrease (ignoring changes in other source categories). In future evaluations of CH_4 isotopic trends, the regional differences in livestock source signatures should be considered.

M-GAS decreased the $\delta^{13}CH_4$ median trend by around 20% from BASE (Fig. 8). The mean natural gas/oil isotopic signature in M-GAS is − 44.5‰, lighter than in BASE (− 40‰). As the emissions of natural gas/oil increased during this period, having a lighter overall natural gas/oil signature leads to a shallower $\delta^{13}CH_4$ trend. M-WET and M-BB both have minimal impacts on the isotopic trend during this decade, likely because the changes in their global mean isotopic signatures from BASE are small.

In the M-ALL simulation regional isotopic signature variability for all five sources was implemented, showing the combined effect of 'M-' simulations. The median M-ALL trend is 30% higher than the BASE trend. Thus the composite impact of the different regional source signatures leads to further disagreement with the NOAA-INSTAAR observations. However, the impact on the trend could be different for other sets of emission inventories. Future studies investigating the CH_4 isotopic trends should consider regional variations in source signatures, which better reflect our knowledge of isotopic signatures than the commonly used global averages.

In every simulation except L-COAL, the simulated isotopic trend is outside the uncertainty range of the observed trend at all sites. This underscores the disagreement of EDGAR v4.2 emissions with observed isotopic trends; under several different isotopic assumptions, the EDGAR coal emissions cannot be reconciled with observations. The isotopic modelling in this paper agrees with atmospheric inversion studies that have doubted the strong increasing trend in the EDGAR coal mining emissions from China (Bergamaschi et al., 2013; Bruhwiler et al., 2014; Peng et al., 2016). However, the assumptions made in this paper should be further tested with more data; for example whether the increase in Chinese coal mining originates from a lower rank of coal, and hence the Chinese coal signature would have become lighter in recent years.

3.4. $\delta^{13}CH_4$ spatial Distribution

The spatial distribution of $\delta^{13}CH_4$ in several simulations is shown in Fig. 9. Source regions can be identified as areas of extreme $\delta^{13}CH_4$, which can differ between the different simulations. For example, a heavy CH_4 signal appears over northeastern China in all of the simulations except for L-COAL. This is an area of high coal emissions, which is a heavy source of methane according to the commonly used signatures (− 35‰). L-COAL assigns coal emissions a lighter isotopic signature (− 50‰), changing the simulated $\delta^{13}CH_4$ in this region.

The interhemispheric difference (IHD) in the simulations is highlighted in Fig. 9 by applying a constant offset to each simulation so that the model agrees with NOAA-INSTAAR observations at Alert, Canada (ALT) (White et al., 2017). The NOAA-INSTAAR observation stations show that Southern Hemisphere (SH) $\delta^{13}CH_4$ is heavier than Northern Hemisphere (NH) $\delta^{13}CH_4$. However, in the BASE simulation NH CH_4 is heavier than SH CH_4. Although this could be due to incorrect distribution of CH_4 emissions in the two hemispheres, incorrect source signature representations could be partly responsible. The $\delta^{13}CH_4$ IHD in BASE has a much larger relative difference from the observed $\delta^{13}CH_4$ IHD than the simulated CH_4 IHD (Section 3.2).

Fig. 10 shows the $\delta^{13}CH_4$ IHD for the simulations and observations, averaged over 2001–2010. Here we defined the IHD as the value at South Pole Observatory (SPO) minus ALT, to simplify comparison with the NOAA-INSTAAR observations. All of the sensitivity simulations display a higher IHD than in BASE, meaning relatively lighter NH CH_4. For each simulation, this could arise in several ways, highlighted in Table 5:

Table 5
Drivers of IHD increases in the sensitivity simulations. The source fractions of total hemispheric CH_4 emissions (e.g. contribution of SH coal to total SH CH_4 emissions) and source signatures are listed for each tested source. The source signatures used in BASE (Table 2) are also listed to highlight global shifts in isotopic signatures. Drivers are either attributed to hemispheric differences in emission fractions, source signatures, or both (see text). Values correspond to the means for the period 2001–2010.

Simulation	Emission Fraction NH* (%)	Emission Fraction SH* (%)	Source Signature NH (%)	Source Signature SH (%)	BASE Source Signature (%)	Driver
L-COAL	10	2	−50	−50	−35	Emission fraction
M-COAL	10	2	−37.9	−42.0	−35	Emission fraction
M-COAL_S	10	2	−39.7	−51.4	−35	Emission fraction
M-WET	21	55	−61.8	−59.4	−59	Source signature
M-BB	2	6	−20.0	−21.8	−21.8	Emission fraction
M-COW	21	16	−65.0	−64.2	−62	Both
M-GAS	20	4	−44.8	−42.9	−40	Both

$$*\text{Emission fraction} = \frac{\text{Emissions from a specific source in a hemisphere}}{\text{Total emissions in a hemisphere}} \times 100\%$$

1. The new source signature is lighter in both hemispheres than in BASE, and the source plays a more important role in the NH than the SH. This is the case for L-COAL, M-COAL, and M-COAL_S. For all of these simulations both hemispheric mean coal signatures were shifted to lighter values from BASE. Since coal mining emissions play a larger role in the NH compared to the SH, lightening the coal signature leads to a relatively lighter NH.
2. The source signature is lighter in the NH than the SH. The M-WET simulation illustrates this effect. NH wetland emissions are lighter than the SH emissions, driving lighter NH CH_4 than in BASE.
3. Reasons 1. and 2. act in concert, leading to increases in the IHD. This occurs for M-COW and M-GAS. In M-COW and M-GAS the livestock and the natural gas/oil signatures in both hemispheres is lighter than in BASE, and the source is more important in the NH, leading to relatively lighter NH CH_4. As well, both of these simulations have a lighter source signature in the NH compared to the SH. M-COW shows a smaller IHD than M-GAS, perhaps because the heavier SH emissions would be concentrated in the tropics, where C_4 vegetation is present (Fig. 3b). Faster tropical interhemispheric transport thus leads to a minimal IHD change for M-COW.
4. The change in IHD from BASE to M-BB is negligible, likely because biomass burning is a relatively minor source in both hemispheres.

As listed above, both the regional distribution of source signatures and the shift in global mean signature can lead to changes in the isotopic IHD. We compare M-WET and M-COW with M-WET_OFFSET and M-COW_OFFSET in Table 6. In the wetlands case, the lighter shift in the wetland isotopic signatures in M-WET only slightly reduces the IHD from M-WET_OFFSET. This is because in M-WET the isotopes are lighter in both hemispheres from BASE, and wetlands are more important relatively in the SH than the NH. The increase in the IHD in the wetlands

Table 6
Comparing the 2001–2010 IHD of M-WET and M-COW (referred to as 'Original simulation' in the table) with M-WET_OFFSET and M-COW_OFFSET (referred to as 'Offset simulation' in the table). The BASE IHD is also listed for comparison.

CH_4 source	Original simulation IHD (%)	Offset simulation IHD (%)
Wetlands	0.08	0.10
Livestock	0.01	0.01
BASE	−0.02	

simulation can therefore be largely attributed to the introduction of lighter boreal wetlands, and not an overall shift in the global mean wetland signature. On the other hand, both M-COW and M-COW_OFFSET show very small IHDs, similar to the BASE IHD. The influence of the livestock signature's regional variability on the IHD is limited because heavier signatures are in the tropics where they are more easily mixed between hemispheres.

None of the sensitivity simulations capture the IHD observed by NOAA-INSTAAR (Fig. 10). However, the combined impacts of the regional source signatures, displayed in the M-ALL simulation, account for 45% of the difference between BASE and observations. This illustrates the importance of source signature representations for the $\delta^{13}CH_4$ spatial distribution. With the emission inventories used here, the spatial variations in the wetland and natural gas/oil signatures play the largest role. Until recently (e.g. Nisbet et al., 2016), regional source signatures had largely been neglected in past research on the $\delta^{13}CH_4$ IHD trends, which only considered changes in emissions (Kai et al., 2011; Levin et al., 2012). The impact of regional source signatures on the IHD is modulated by the choice of emission inventory. For example,

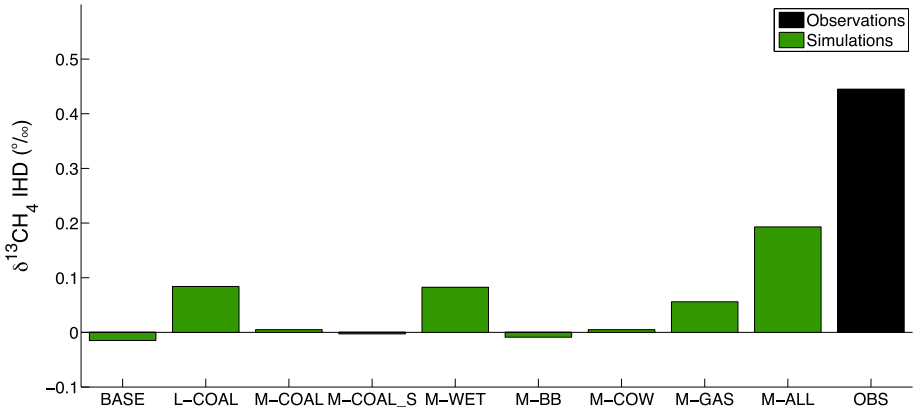

Fig. 10. Interhemispheric difference (SH minus NH) of $\delta^{13}CH_4$ calculated in the isotopic signature sensitivity simulations and NOAA-INSTAAR using values at South Pole Observatory (SPO) and ALT for 2001–2010.

employing the same assumptions as M-WET for a wetland model with higher boreal CH_4 emissions would further increase the IHD, because NH wetlands would be even lighter. Uncertainties in emissions likely account for the remaining gap between observed and simulated IHD. Transport errors are expected to play a more minor role, as the model under specified dynamics can accurately represent the CH_4 IHD (Fig. 5).

Sensitivity studies were not performed on the influence of sink fractionation on the isotopic trends and spatial distributions. Fractionation factors for CH_4 sinks have been measured by several groups with relatively good agreement (Feilberg et al., 2005; Saueressig et al., 2001; Tyler et al., 2000; Crowley et al., 1999; Roberto-Neto et al., 1998; Saueressig et al., 1995; Cantrell et al., 1990). However, the spatial distribution and temporal trend of the OH sink remain a source of uncertainty. Sinks can alter the spatial distribution of CH_4 isotopes, as part of the observed isotopic enrichment of the SH is due to sink fractionation during transport of CH_4 from the NH to the SH (Quay et al., 1999). The isotopic effect of changing OH distributions and trends could be a subject of further research.

4. Conclusions

Whereas other studies have focused on the impacts of emissions on CH_4 isotopic trends and spatial distribution, we have investigated the influences of source signature representation on CH_4 isotopes. Regional source signatures for coal, natural gas/oil, wetlands, livestock, and biomass burning were developed and implemented based on the available literature. The newly calculated global mean isotopic signatures are in general lighter than previous estimations. Two methods for representing the regional coal signatures lead to different isotopic trends, revealing that more measurements of coal isotopic signatures are necessary. Introducing regionally distinct signatures for C_3 and C_4 fed-livestock leads to an 14% higher $\delta^{13}CH_4$ trend during 2003–2010 compared to using a global average livestock signature. This means that larger increases in tropical livestock emissions would be needed to explain the $\delta^{13}CH_4$ decrease after 2008, compared to what would be expected from a global average livestock source signature. The combination of all of the regional source signatures leads to a stronger increasing $\delta^{13}CH_4$ trend as with the commonly used isotopic signatures. We show that the Chinese coal emission increase in EDGAR v4.2 is difficult to reconcile with observed NOAA-INSTAAR $\delta^{13}CH_4$ trends, unless China has increased production of lower grade coal with a lighter source signature. Including regional source signatures also has a large impact on the $\delta^{13}CH_4$ spatial distribution, accounting for 45% of the $\delta^{13}CH_4$ IHD gap between simulations and observations. As CH_4 emissions have changed distinctly in different regions, we think that it is important to capture the regional character of source signatures in future modelling studies. Further field and laboratory measurements of the $\delta^{13}CH_4$ of emissions are essential to refine our estimates of regional source signatures.

Acknowledgements

Thanks to researchers at both NOAA-ESRL for use of their CH_4 measurements and INSTAAR at University of Colorado for use of their isotopic CH_4 observations. Sylvia Michel and Ed Dlugokencky provided useful information about these measurements. Discussions with Euan Nisbet and David Lowry of Royal Holloway, University of London and Giulia Zazzeri of Imperial College London on CH_4 isotopic source signatures were very helpful. Support for this study was provided by the Competence Center Environment and Sustainability (CCES) at ETH, within the MAIOLICA-2 project (42-01).

Appendix A. Supplementary data

Supplementary data related to this article can be found at http://dx.doi.org/10.1016/j.atmosenv.2017.11.037.

References

Allan, W., Manning, M., Lassey, K., Lowe, D., Gomez, A., 2001. Modeling the variation of $\delta^{13}C$ in atmospheric methane: phase ellipses and the kinetic isotope effect. Glob. Biogeochem. Cycles 15 (2), 467–481.

Allan, W., Struthers, H., Lowe, D., 2007. Methane carbon isotope effects caused by atomic chlorine in the marine boundary layer: global model results compared with southern hemisphere measurements. J. Geophys. Res. Atmos. 112 (D4).

Allègre, C., Sutcliffe, C., 2008. Isotope Geology. Cambridge University Press.

Bergamaschi, P., Houweling, S., Segers, A., Krol, M., Frankenberg, C., Scheepmaker, R., Dlugokencky, E., Wofsy, S., Kort, E., Sweeney, C., et al., 2013. Atmospheric CH_4 in the first decade of the 21st century: inverse modeling analysis using SCIAMACHY satellite retrievals and NOAA surface measurements. J. Geophys. Res. Atmos. 118 (13), 7350–7369.

Bloom, A., Palmer, P., Fraser, A., Reay, D., Frankenberg, C., 2010. Large-scale controls of methanogenesis inferred from methane and gravity spaceborne data. Science 327 (5963), 322–325.

Bousquet, P., Ringeval, B., Pison, I., Dlugokencky, E., Brunke, E.-G., Carouge, C., Chevallier, F., Fortems-Cheiney, A., Frankenberg, C., Hauglustaine, D., et al., 2011. Source attribution of the changes in atmospheric methane for 2006–2008. Atmos. Chem. Phys. 11 (8), 3689–3700.

Brownlow, R., Lowry, D., Fisher, R., France, J., Lanoisellé, M., White, B., Wooster, M., Zhang, T., Nisbet, E., 2017. Isotopic ratios of tropical methane emissions by atmospheric measurement. Glob. Biogeochem. Cycles 31 (9), 1408–1419.

Bruhwiler, L., Dlugokencky, E., Masarie, K., Ishizawa, M., Andrews, A., Miller, J., Sweeney, C., Tans, P., Worthy, D., 2014. CarbonTracker-CH_4: an assimilation system for estimating emissions of atmospheric methane. Atmos. Chem. Phys. 14 (16), 8269–8293.

Cantrell, C., Shetter, R., McDaniel, A., Calvert, J., Davidson, J., Lowe, D., Tyler, S., Cicerone, R., Greenberg, J., 1990. Carbon kinetic isotope effect in the oxidation of methane by the hydroxyl radical. J. Geophys. Res. Atmos. 95 (D13), 22455–22462.

Coulon, A., 2016. The Drivers of Atmospheric Methane Fluctuations Over the Last Three Decades. Ph.D. thesis. ETH Zürich Open access. https://doi.org/10.3929/ethz-b-000170678.

Crowley, J., Saueressig, G., Bergamaschi, P., Fischer, H., Harris, G., 1999. Carbon kinetic isotope effect in the reaction CH_4 + Cl: a relative rate study using FTIR spectroscopy. Chem. Phys. Lett. 303 (3), 268–274.

Dee, D., Uppala, S., Simmons, A., Berrisford, P., Poli, P., Kobayashi, S., Andrae, U., Balmaseda, M., Balsamo, G., Bauer, P., Bechtold, P., Beljaars, A.C., van de Berg, L., Bidlot, J., Bormann, N., Delsol, C., Dragani, R., Fuentes, M., Geer, A., Haimberger, L., Healy, S., Hersbach, H., Hlm, E., Isaksen, L., Kllberg, P., Khler, M., Matricardi, M., McNally, A., Monge-Sanz, B., Morcrette, J., Park, B., Peubey, C., de Rosnay, P., Tavolato, C., Thpaut, J., Vitart, F., 2011. The ERA-Interim reanalysis: configuration and performance of the data assimilation system. Q. J. R. Meteorol. Soc. 137 (656), 553–597.

Dlugokencky, E., Bruhwiler, L., White, J., Emmons, L., Novelli, P.C., Montzka, S.A., Masarie, K.A., Lang, P.M., Crotwell, A., Miller, J.B., et al., 2009. Observational constraints on recent increases in the atmospheric CH_4 burden. Geophys. Res. Lett. 36 (18).

Dlugokencky, E., Lang, P., Crotwell, A., Masarie, K., Crotwell, M., 2015. Atmospheric Methane Dry Air Mole Fractions from the NOAA ESRL Carbon Cycle Cooperative Global Air Sampling Network, 1983-2014, Version: 2015-08-03. Path. ftp://aftp.cmdl.noaa.gov/data/trace_gases/ch4/flask/surface/.

Dlugokencky, E., Nisbet, E., Fisher, R., Lowry, D., 2011. Global atmospheric methane: budget, changes and dangers. Phil. Trans. Roy. Soc. Lond. A Math. Phys. Eng. Sci. 369 (1943), 2058–2072.

EDGAR, 2011. Emission Database for Global Atmospheric Research (EDGAR), Release Version 4.2. European Commission, Joint Research Centre (JRC)/Netherlands Environmental Assessment Agency (PBL), Ispra, Italy. http://edgar.jrc.ec.europa.eu/index.php.

Egorova, T., Rozanov, E., Zubov, V., Karol, I., 2003. Model for investigating ozone trends (MEZON). Izvestiya Atmos. Ocean. Phys. 39 (3), 277–292.

Etiope, G., Milkov, A.V., 2004. A new estimate of global methane flux from onshore and shallow submarine mud volcanoes to the atmosphere. Environ. Geol. 46 (8), 997–1002.

Etminan, M., Myhre, G., Highwood, E., Shine, K., 2016. Radiative forcing of carbon dioxide, methane, and nitrous oxide: a significant revision of the methane radiative forcing. Geophys. Res. Lett. 43 (24).

Euracoal, 2011. Coal industry across Europe 2011. https://euracoal.eu/library/publications/.

Feilberg, K., Griffith, D., Johnson, M., Nielsen, C., 2005. The ^{13}C and D kinetic isotope effects in the reaction of CH_4 with Cl. Int. J. Chem. Kinet. 37 (2), 110–118.

Fisher, R., France, J., Lowry, D., Lanoisellé, M., Brownlow, R., Pyle, J., Cain, M., Warwick, N., Skiba, U., Drewer, J., et al., 2017. Measurement of the 13c isotopic signature of methane emissions from northern European wetlands. Glob. Biogeochem. Cycles 31 (3), 605–623.

Fung, I., John, J., Lerner, J., Matthews, E., Prather, M., Steele, L., Fraser, P., 1991. Three-dimensional model synthesis of the global methane cycle. J. Geophys. Res. Atmos. 96 (D7), 13033–13065.

Ghosh, A., Patra, P., Ishijima, K., Umezawa, T., Ito, A., Etheridge, D., Sugawara, S., Kawamura, K., Miller, J., Dlugokencky, E., et al., 2015. Variations in global methane sources and sinks during 1910–2010. Atmos. Chem. Phys. 15 (5), 2595–2612.

Gros, V., Brenninkmeijer, C., Jöckel, P., Kaiser, J., Lowry, D., Nisbet, E., OBrien, P., Röckmann, T., Warwick, N., 2004. Use of isotopes. In: Emissions of Atmospheric Trace Compounds. Springer, pp. 361–426.

Hartmann, D., Klein Tank, A., Rusicucci, M., Alexander, L., Broenniman, B., Charabi, Y., Dentener, F., Dlugokencky, E., Easterling, D., Kaplan, A., et al., 2013. Observations: atmosphere and surface. In: Climate Change 2013: the Physical Science Basis. Contribution of Working Group I to the Fifth Assessment Report of the Intergovernmental Panel on Climate Change. Cambridge University Press, pp. 159–254.

Hausmann, P., Sussmann, R., Smale, D., 2016. Contribution of oil and natural gas production to renewed increase in atmospheric methane (2007–2014): top–down estimate from ethane and methane column observations. Atmos. Chem. Phys. 16 (5), 3227–3244.

Hodson, E., Poulter, B., Zimmermann, N., Prigent, C., Kaplan, J., 2011. The El Niño–Southern Oscillation and wetland methane interannual variability. Geophys. Res. Lett. 38 (8).

Hosgörmez, H., 2007. Origin and secondary alteration of coalbed and adjacent rock gases in the Zonguldak Basin, western Black Sea Turkey. Geochem. J. 41 (3), 201–211.

Houweling, S., Kaminski, T., Dentener, F., Lelieveld, J., Heimann, M., 1999. Inverse modeling of methane sources and sinks using the adjoint of a global transport model. J. Geophys. Res. Atmos. 104 (D21), 26137–26160.

IEA, 2015. Outheast Asia Energy Outlook 2015: World Energy Outlook Special Report. https://www.iea.org/publications/freepublications/publication/weo2015_Ω-southeastasia.pdf.

Kai, F., Tyler, S., Randerson, J., Blake, D., 2011. Reduced methane growth rate explained by decreased Northern Hemisphere microbial sources. Nature 476 (7359), 194–197.

Kanduč, T., Grassa, F., Lazar, J., Zavšek, S., 2015. Geochemical and isotopic characterization of coalbed gases in active excavation fields at Preloge and Pesje (Velenje Basin) mining areas. RMZ–M&G 62, 21–36.

Kirschke, S., Bousquet, P., Ciais, P., Saunois, M., Canadell, J., Dlugokencky, E., Bergamaschi, P., Bergmann, D., Blake, D., Bruhwiler, L., et al., 2013. Three decades of global methane sources and sinks. Nat. Geosci. 6 (10), 813–823.

Koplitz, S., Jacob, D., Sulprizio, M., Myllyvirta, L., Reid, C., 2017. Burden of disease from rising coal-fired power plant emissions in Southeast Asia. Environ. Sci. Technol. 51 (3), 1467–1476.

Lambert, G., Schmidt, S., 1993. Reevaluation of the oceanic flux of methane: uncertainties and long term variations. Chemosphere 26 (1–4), 579–589.

Lassey, K., Etheridge, D., Lowe, D., Smith, A., Ferretti, D., 2007. Centennial evolution of the atmospheric methane budget: what do the carbon isotopes tell us? Atmos. Chem. Phys. 7 (8), 2119–2139.

Levin, I., Veidt, C., Vaughn, B., Brailsford, G., Bromley, T., Heinz, R., Lowe, D., Miller, J., Poß, C., White, J., 2012. No inter-hemispheric 13CH4 trend observed. Nature 486 (7404), E3–E4.

Lin, S., Rood, R.B., 1996. Multidimensional flux-form semi-Lagrangian transport schemes. Mon. Weather Rev. 124 (9), 2046–2070.

Martens, C., Kelley, C., Chanton, J., Showers, W., 1992. Carbon and hydrogen isotopic characterization of methane from wetlands and lakes of the Yukon-Kuskokwim Delta, western Alaska. J. Geophys. Res. Atmos. 97 (D15), 16689–16701.

McCalley, C., Woodcroft, B., Hodgkins, S., Wehr, R., Kim, E., Mondav, R., Crill, P., Chanton, J., Rich, v., Tyson, G., et al., 2014. Methane dynamics regulated by microbial community response to permafrost thaw. Nature 514 (7523), 478–481.

Monteil, G., Houweling, S., Dlugockenky, E., Maenhout, G., Vaughn, B., White, J., Rockmann, T., 2011. Interpreting methane variations in the past two decades using measurements of CH_4 mixing ratio and isotopic composition. Atmos. Chem. Phys. 11 (17), 9141–9153.

Montzka, S., Krol, M., Dlugokencky, E., Hall, B., Jöckel, P., Lelieveld, J., 2011. Small interannual variability of global atmospheric hydroxyl. Science 331 (6013), 67–69.

Nakazawa, T., Ishizawa, M., Higuchi, K., Trivett, N., 1997. Two curve fitting methods applied to CO_2 flask data. Environmetrics 8 (3), 197–218.

Nisbet, E., Dlugokencky, E., Bousquet, P., 2014. Methane on the rise–again. Science 343 (6170), 493–495.

Nisbet, E., Dlugokencky, E., Manning, M., Lowry, D., Fisher, R., France, J., Michel, S., Miller, J., White, J., Vaughn, B., Bousquet, P., Pyle, J., Warwick, N., Cain, M., Brownlow, R., Zazzeri, G., Lanoisellé, M., Manning, A., Gloor, E., Worthy, D., Brunke, E., Labuschagne, C., Wolff, E., Ganesan, A., 2016. Rising atmospheric methane: 2007-2014 growth and isotopic shift. Glob. Biogeochem. Cycles 30 (9), 1356–1370.

O'Shea, S., Allen, G., Gallagher, M., Bower, K., Illingworth, S., Muller, J., Jones, B., Percival, C., Bauguitte, S., Cain, M., et al., 2014. Methane and carbon dioxide fluxes and their regional scalability for the European Arctic wetlands during the MAMM project in summer 2012. Atmos. Chem. Phys. 14 (23), 13159–13174.

Patra, P., Houweling, S., Krol, M., Bousquet, P., Belikov, D., Bergmann, D., Bian, H., Cameron-Smith, P., Chipperfield, M., Corbin, K., et al., 2011. TransCom model simulations of CH_4 and related species: linking transport, surface flux and chemical loss with CH_4 variability in the troposphere and lower stratosphere. Atmos. Chem. Phys. 11 (24), 12813–12837.

Patra, P., Krol, M., Montzka, S., Arnold, T., Atlas, E., Lintner, B., Stephens, B., Xiang, B., Elkins, J., Fraser, P., et al., 2014. Observational evidence for interhemispheric hydroxyl-radical parity. Nature 513 (7517), 219–223.

Patra, P., Saeki, T., Dlugokencky, E., Ishijima, K., Umezawa, T., Ito, A., Aoki, S., Morimoto, S., Kort, E., Crotwell, A., et al., 2016. Regional emission and loss budgets of atmospheric methane (2002-2012). J. Meteorol. Soc. Jpn. 94, 83–105.

Peng, S., Piao, S., Bousquet, P., Ciais, P., Li, B., Lin, X., Tao, S., Wang, Z., Zhang, Y., Zhou, F., 2016. Inventory of anthropogenic methane emissions in mainland China from 1980 to 2010. Atmos. Chem. Phys. 16 (22), 14545–14562.

Pöschl, U., von Kuhlmann, R., Poisson, N., Crutzen, P., 2000. Development and intercomparison of condensed isoprene oxidation mechanisms for global atmospheric modeling. J. Atmos. Chem. 37 (1), 29–52.

Quay, P., Stutsman, J., Wilbur, D., Snover, A., Dlugokencky, E., Brown, T., 1999. The isotopic composition of atmospheric methane. Glob. Biogeochem. Cycles 13 (2), 445–461.

Randerson, J., Chen, Y., Werf, G., Rogers, B., Morton, D., 2012. Global burned area and biomass burning emissions from small fires. J. Geophys. Res. Biogeosciences 117 (G4) 2005–2012.

Randerson, J., Van der Werf, G., Collatz, G., Giglio, L., Still, C., Kasibhatla, P., Miller, J., White, J., DeFries, R., Kasischke, E., 2005. Fire emissions from C3 and C4 vegetation and their influence on interannual variability of atmospheric CO_2 and $\delta^{13}CO_2$. Glob. Biogeochem. Cycles 19 (2).

Revell, L., Tummon, F., Stenke, A., Sukhodolov, T., Coulon, A., Rozanov, E., Garny, H., Grewe, V., Peter, T., 2015. Drivers of the tropospheric ozone budget throughout the 21st century under the medium-high climate scenario RCP 6.0. Atmos. Chem. Phys. 15 (10), 5887–5902.

Rice, A., Butenhoff, C., Teama, D., Röger, F., Khalil, M., Rasmussen, R., 2016. Atmospheric methane isotopic record favors fossil sources flat in 1980s and 1990s with recent increase. Proc. Natl. Acad. Sci. 113 (39), 10791–10796.

Rigby, M., Montzka, S., Prinn, R., White, J., Young, D., ODoherty, S., Lunt, M., Ganesan, A., Manning, A., Simmonds, P., et al., 2017. Role of atmospheric oxidation in recent methane growth. Proc. Natl. Acad. Sci. 114 (21), 5373–5377.

Roberto-Neto, O., Coitiño, E., Truhlar, D., 1998. Dual-level direct dynamics calculations of deuterium and carbon-13 kinetic isotope effects for the reaction $Cl + CH_4$. J. Phys. Chem. A 102 (24), 4568–4578.

Roeckner, E., Bäuml, G., Bonaventura, L., Brokopf, R., Esch, M., Giorgetta, M., Hagemann, S., Kirchner, I., Kornblueh, L., Manzini, E., et al., 2003. The Atmospheric General Circulation Model ECHAM 5. PART I: Model Description.

Rust, F., 1981. Ruminant methane $\delta(^{13}C/^{12}C)$ values: relation to atmospheric methane. Science 211 (4486), 1044–1046.

Saueressig, G., Bergamaschi, P., Crowley, J., Fischer, H., Harris, G., 1995. Carbon Kinetic Isotope Effect of the Reaction of CH4 with Cl Atoms.

Saueressig, G., Crowley, J., Bergamaschi, P., Brühl, C., Brenninkmeijer, C., Fischer, H., 2001. Carbon 13 and D kinetic isotope effects in the reactions of CH_4 with $O(^1D)$ and OH: New laboratory measurements and their implications for the isotopic composition of stratospheric methane. J. Geophys. Res. Atmos. 106 (D19), 23127–23138 1984–2012.

Saunois, M., Bousquet, P., Poulter, B., Peregon, A., Ciais, P., Canadell, J., Dlugokencky, E., Etiope, G., Bastviken, D., Houweling, S., et al., 2016. The global methane budget 2000-2012. Earth Syst. Sci. Data 8 (2), 697.

Schaefer, H., Fletcher, S., Veidt, C., Lassey, K., Brailsford, G., Bromley, T., Dlugokencky, E., Michel, S., Miller, J., Levin, I., et al., 2016. A 21st-century shift from fossil-fuel to biogenic methane emissions indicated by $^{13}CH_4$. Science 352 (6281), 80–84.

Schultz, M., Rast, S., 2007. Emission data sets and methodologies for estimating emissions. http://retro-archive.iek.fz-juelich.de/data/documents/reports/D1-6_final.pdf REanalysis of the TROpospheric chemical composition over the past 40 years, A long-term global modeling study of tropospheric chemistry funded under the 5th EU framework programme. Tech. rep.

Schwietzke, S., Griffin, W., Matthews, H., Bruhwiler, L., 2014. Global bottom-up fossil fuel fugitive methane and ethane emissions inventory for atmospheric modeling. ACS Sustain. Chem. Eng. 2 (8), 1992–2001.

Schwietzke, S., Sherwood, O., Bruhwiler, L., Miller, J., Etiope, G., Dlugokencky, E., Michel, S., Arling, V., Vaughn, B., White, J., et al., 2016. Upward revision of global fossil fuel methane emissions based on isotope database. Nature 538 (7623), 88–91.

Sherwood, O., Schwietzke, S., Arling, V., Etiope, G., 2016. Global Inventory of Fossil and Non-fossil Methane $\delta^{13}C$ Source Signature Measurements for Improved Atmospheric Modeling. http://www.esrl.noaa.gov/gmd/ccgg/d13C-src-inv/.

Snover, A., Quay, P., 2000. Hydrogen and carbon kinetic isotope effects during soil uptake of atmospheric methane. Glob. Biogeochem. Cycles 14 (1), 25–39.

Spahni, R., Wania, R., Neef, L., Weele, M. v., Pison, I., Bousquet, P., Frankenberg, C., Foster, P., Joos, F., Prentice, I., et al., 2011. Constraining global methane emissions and uptake by ecosystems. Biogeosciences 8 (6), 1643–1665.

Stenke, A., Schraner, M., Rozanov, E., Egorova, T., Luo, B., Peter, T., 2013. The SOCOL version 3.0 chemistry–climate model: description, evaluation, and implications from an advanced transport algorithm. Geosci. Model Dev. 6 (5), 1407–1427.

Still, C., Berry, J., Collatz, G., DeFries, R., 2003. Global distribution of C3 and C4 vegetation: carbon cycle implications. Glob. Biogeochem. Cycles 17 (1).

Tans, P., 1997. A note on isotopic ratios and the global atmospheric methane budget. Glob. Biogeochem. Cycles 11 (1), 77–81.

Turner, A., Frankenberg, C., Wennberg, P., Jacob, D., 2017. Ambiguity in the causes for decadal trends in atmospheric methane and hydroxyl. Proc. Natl. Acad. Sci. 201616020.

Tyler, S., 1986. Stable carbon isotope ratios in atmospheric methane and some of its sources. J. Geophys. Res. Atmos. 91 (D12), 13232–13238.

Tyler, S., Ajie, H., Rice, A., Cicerone, R., Tuazon, E., 2000. Experimentally determined kinetic isotope effects in the reaction of CH_4 with Cl: implications for atmospheric CH_4. Geophys. Res. Lett. 27 (12), 1715–1718.

Tyler, S., Rice, A., Ajie, H., 2007. Stable isotope ratios in atmospheric CH_4: implications for seasonal sources and sinks. J. Geophys. Res. Atmos. 112 (D3).

Tyler, S., Zimmerman, P., Cumberbatch, C., Greenberg, J., Westberg, C., Darlington, J., 1988. Measurements and interpretation of $\delta^{13}C$ of methane from termites, rice paddies, and wetlands in Kenya. Glob. Biogeochem. Cycles 2 (4), 341–355.

Umezawa, T., Machida, T., Aoki, S., Nakazawa, T., 2012. Contributions of natural and anthropogenic sources to atmospheric methane variations over western Siberia estimated from its carbon and hydrogen isotopes. Glob. Biogeochem. Cycles 26 (4).

Walter, K., Chanton, J., Chapin, F., Schuur, E., Zimov, S., 2008. Methane production and bubble emissions from arctic lakes: isotopic implications for source pathways and ages. J. Geophys. Res. Biogeosciences 113 (G3).

Walter, K., Zimov, S., Chanton, J., Verbyla, D., Chapin III, F., 2006. Methane bubbling from Siberian thaw lakes as a positive feedback to climate warming. Nature 443

(7107), 71–75.
White, J., Vaughn, B., Michel, S., 2017. Institute of Arctic and Alpine Research (INSTAAR), Stable Isotopic Composition of Atmospheric Methane (13C) from the NOAA ESRL Carbon Cycle Cooperative Global Air Sampling Network, 1998-2015, Version: 2017-01-20. Path. University of Colorado. ftp://aftp.cmdl.noaa.gov/data/trace_gases/ch4c13/flask/.
World Energy Council, 2007. Survey of Energy Resources.
Zazzeri, G., Lowry, D., Fisher, R., France, J., Lanoisellé, M., Kelly, B., Necki, J., Iverach, C., Ginty, E., Zimnoch, M., Jasek, A., Nisbet, E., 2016. Carbon isotopic signature of coal-derived methane emissions to the atmosphere: from coalification to alteration. Atmos. Chem. Phys. 16 (21), 13669–13680.
Zazzeri, G., Lowry, D., Fisher, R., France, J., Lanoisellé, M., Nisbet, E., 2015. Plume mapping and isotopic characterisation of anthropogenic methane sources. Atmos. Environ. 110, 151–162.
Zhang, Z., Zimmermann, N., Kaplan, J., Poulter, B., 2016. Modeling spatiotemporal dynamics of global wetlands: comprehensive evaluation of a new sub-grid TOPMODEL parameterization and uncertainties. Biogeosciences 13 (5), 1387–1408.
Zhu, W., 2013. Coal to surpass gas in Southeast Asia power boom. https://www.bloomberg.com/news/articles/2013-10-02/coal-to-surpass-gas-in-southeast-asia-power-use-boom-iea-says.